RSC Advances

ROYAL SOCIETY OF CHEMISTRY

www.rsc.org/advances

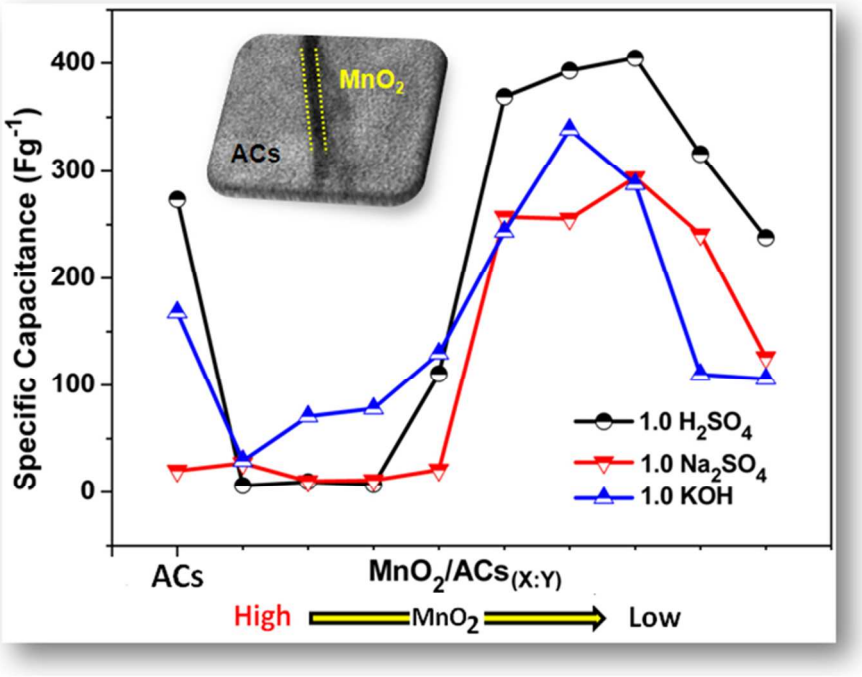

Efficient needle-like MnO2/activated carbon nanocomposites have been prepared and demonstrated as versatile electrode materials for supercapacitors
254x190mm (96 x 96 DPI)

RSC Advances

ARTICLE

Needle-like MnO_2/activated carbon nanocomposites derived from human hair as versatile electrode materials for supercapacitors

Received 00th January 20xx,
Accepted 00th January 20xx

DOI: 10.1039/x0xx00000x

www.rsc.org/

Dian Deng,[a] Byoung-Suhk Kim,[b] Mayakrishnan Gopiraman[a,*] Ick Soo Kim[a,*]

Bio-waste material, human hair, was used as a source to prepare activated carbon (ACs) by a simple NaOH activation method. MnO_2 with needle like structure was successfully decorated on ACs by wet impregnation method. TEM images confirmed needle-like morphology of MnO_2 on ACs. The chemical state of MnO_2 was found to be +4, as confirmed by XPS analysis. Other physicochemical properties of MnO_2/ACs were investigated by means of SEM-EDS, XRD, Raman and XPS analyses. After complete characterization, the resultant nanocomposites with different MnO_2-loading [$MnO_2/ACs_{(X:Y)}$] were employed as electrode materials for supercapacitor. Interestingly, the MnO_2/ACs nanocomposites showed an excellent capacitance in three different electrolytes (1.0 M H_2SO_4, 1.0 M KOH and 1.0 M Na_2SO_4). The $MnO_2/ACs_{(1:12)}$ achieved a maximum capacitance of 410 F/g, 345 F/g and 291 F/g in 1.0 M H_2SO_4, 1.0 KOH and 1.0 Na_2SO_4, respectively. To the best of our knowledge, this is the first MnO_2-based carbon nanocomposite to show good capacitance performance in three different kinds of electrolytes. Moreover, the MnO_2/ACs showed capacitance of ~300 F/g even after 500 cycles in 1.0 M H_2SO_4.

1. Introduction

Supercapacitors have recently gained huge attention due to their advantages such as longer cycle life, short charging time and higher power density compared to conventional electrical double-layer capacitors.[1] Several carbon-based electrode materials such as activated carbon (ACs), graphene, carbon nanotubes (CNTs), fullerenes, and carbon fibers are reported as superior supercapacitor electrode materials.[2,3] Among them, due to low cost, very high specific surface area and pore properties, ACs are often preferable over other carbon materials.[4] Recently, Qian *et al.*,[5] prepared carbon flakes from human hair and employed as electrode materials for supercapacitors. They found that the carbon flakes have a very high specific capacitance of 340 F g^{-1} in 6.0 M KOH at a current density of 1 A g^{-1} and good stability over 20000 cycles. Alike, Ma and co-workers[6] used cotton fiber as carbon source to prepare porous activated carbon (PACs). As an electrode material, the prepared PACs showed a high specific capacitance of 239 F g^{-1} at 0.5 A g^{-1} current density and good rate capability in 2.0 M KOH aqueous electrolyte. Alike, ACs derived from plant leaves exhibited a specific capacitance of 400 F g^{-1} and an energy density of 55 Wh Kg^{-1} in 1.0 M H_2SO_4.[7] Most of the ACs derived from biomass is performed as electrode materials either in acid or base electrolyte.[8,9] However, the drawback of these ACs is its poor capacitance performance in neutral electrolytes such as Na_2SO_4 and K_2SO_4; only a very few reports exist up to now on the capacitance performance of ACs in neutral electrolytes.[10] Hence, the development of a versatile supercapacitor electrode material (which can perform in various electrolytes such as acid, base and neutral media) is a challenging task.

Modification or functionalization of porous ACs with metal oxides such as MnO_x, RuO_x, NiO_x and CuO_x is one of the promising approaches to achieve superior electrode performance.[11,12] Among them, manganese oxide (MnO_2) is often preferred as an electrode material for supercapacitors due the low cost, high theoretical surface area and non-toxic.[13] Moreover, the MnO_2 can exhibit larger capacitance values and energy density due to its fast surface redox reactions. The MnO_2 has showed a maximum specific capacitance of 1370 F/g^{-1}.[14] However, the pseudocapacitive reaction of MnO_2 is known to be a surface reaction that can occur only on the surface. Hence, the MnO_2 is often combined with conductive materials such as graphene, CNTs and carbon fibers to improve its performance.[15] Yan *et al.*,[16] prepared MnO_2/graphene and employed as supercapacitor electrode material. The MnO_2/graphene demonstrated a very high capacitance of 310 F/g. MnO_2 nanorods were supported on ACs and employed as electrode material for supercapacitor.[17] It showed a moderate capacitance of 165 F/g in Na_2SO_4 electrolyte. In case of MnO_2/activated carbon composites, the performance is mainly dependent on five factors:[18,19] (a) surface area of the

[a] *Nano Fusion Technology Research Lab, Interdisciplinary Cluster for Cutting Edge Research (ICCER), Division of Frontier Fibers, Institute for Fiber Engineering (IFES), National University Corporation, Shinshu University, Ueda, Nagano, 386-8567, Japan.E-mail addresses: kim@shinshu-u.ac.jp (I.S. Kim) and gopiramannitt@gmail.com (M. Gopiraman).*
[b] *Department of Organic Materials & Fiber Engineering, Chonbuk National University, 567 Baekje-daero, Deokjin-gu, Jeonju-si, Jeollabuk-do 561-756, Republic of Korea.*

Electronic Supplementary Information (ESI) available: SEM images, EDS spectra, BET isotherm curves and XRD spectra are provided. See DOI: 10.1039/x0xx00000x

composites, (b) structure of the MnO_2 and ACs, (c) conductivity of the materials, (d) large pore volume and pore size, and (e) presence of heteroatom such as O, N and S. Recently, human hair has been used to prepare ACs with very high surface area and excellent pore structure. In addition, the ACs found to consist of various heteroatoms such as O, N and S, and has exhibited very high specific capacitance in 6 M KOH electrolyte.[5] We believe that the functionalization of MnO_2 with unique structure on ACs (derived from human hair) would show superior capacitance performance in various electrolytes.

Herein, we prepared needle-like MnO_2/ACs nanocomposites with different MnO_2 loading by a simple wet impregnation method. The ACs was derived from human hair by NaOH activation. The prepared composite materials were characterized by various spectroscopic and microscopic methods such as HR-TEM, SEM-EDS, XRD, Raman and XPS analyses. After complete characterization, the resultant nanocomposites $MnO_2/ACs_{(X:Y)}$] were employed as electrode materials for supercapacitor in three different electrolytes, namely, 1.0 M H_2SO_4, 1.0 M KOH and 1.0 M Na_2SO_4. Conductivity and cycle life of the nanocomposites were also studied.

2. Experimental

2.1 Materials

Human hair was collected from students of Shinshu University, Japan. Nafion®perfluorinated resin solution (5 wt%), 2-propanol, potassium permanganate ($KMnO_4$) were purchased from Sigma Aldrich. Sodium sulfate (Na_2SO_4), potassium hydroxide (KOH), sulfuric acid (H_2SO_4), hydrochloric acid (HCl) and sodium hydroxide (NaOH) were purchased from Wako Pure Chemicals, Japan. All chemicals were used without further purification.

2.2 Preparation of ACs

The ACs was prepared from human hair according to the previously reported procedure.[5] In a typical experiment, 1.0 g of human hair was washed well and dried in air. At first, the human hair was stabilized under air atmosphere at 300°C (heating rate of 1°C/min) for 1 h. Subsequently, the stabilized human hair was mixed with NaOH (human hair/NaOH = 1:2 ratio) using mortar and pestle until the homogeneous mixture was obtained. Finally, the mixture was calcinated in the muffle furnace under N_2 atmosphere at 700°C (heating rate of 5°C/min) for 3 h. After calcination, the resultant solid was washed well with 1 M HCl to remove the NaOH.

2.3 Synthesis of $MnO_2/ACs_{(X:Y)}$ nanocomposites

In a typical synthesis procedure, 25 mg of ACs was dispersed in 10 mL distilled water followed by sonication for 30 min. To the above mixture, $KMnO_4$ solution was added drop by drop under vigorous stirring condition. After the addition of $KMnO_4$, the mixture was stirred at 60°C for 24 h and then vacuum filtered to obtain the MnO_2/ACs. ACs and $KMnO_4$ with different weight ratios (ACs/$KMnO_4$ = 1:2, 1:1, 2:1, 4:1, 8:1, 10:1, 12:1, 14:1 and 16:1) were prepared. Here, the nanocomposites are denoted as $MnO_2/ACs_{(X:Y)}$, where X is the weight ratio of ACs and Y represents the weight ratio of $KMnO_4$. Finally, the MnO_2/ACs was washed well with water and air dried. The resultant composites were characterized in detail and used for electrochemical studies.

2.4 Characterization

The surface morphology of the resultant MnO_2/ACs composites was studied by field emission scanning electron microscopy (FE-SEM; S-5000, Hitachi) and transmission electron microscopy (TEM; 2010FasTEM, JEOL, Japan). Energy dispersive X-ray spectra (EDS) were performed on JEOL JSM-5900. X-ray photoelectron spectroscopy (XPS; AXIS-ULTRADLD, Shimadzu) and Raman spectrometer (Hololab 5000, Kaiser Optical Systems, Inc., Ann Arbor, MI, USA) were recorded to study the chemical state of the atoms presented in the MnO_2/ACs. X-ray diffraction (XRD) experiment was performed at 27°C using a Rotaflex RTP300 (Rigaku Co., Japan) diffractometer at 50 kV and 200 mA with a scan speed of 2°/min. Nickel-filtered Cu K_α radiation ($5<2\theta<70^o$) was used for XRD measurements. For Raman analysis, Ar laser was operated at 532 nm with a Kaiser holographic edge filter. The specific surface area of samples was determined using the Brunauer-Emmett-Teller (BET) method (BELSORP-max, BEL Japan, Inc.). The electrochemical studies were carried out in Versastat-4 potentiostat at a scan rate ranging from 5 to 100 mV/s.

2.5 Electrochemical measurements

The electrochemical measurements were carried out in three different electrolytes (1.0 M H_2SO_4, 1.0 M KOH and 1.0 M Na_2SO_4) at 27°C using Versastat 4 electrochemical station. The sweep potential range was adjusted from -0.2 to 0.8 V [vs. Ag/AgCl] in an electrochemical cell with three-electrode system: platinum wire, Ag/AgCl and prepared carbon nanocomposites were used as counter electrode, reference electrode and working electrode, respectively. The electrochemical impedance spectroscopy (EIS) was recorded in the frequency range of 0.01 Hz to 100 kHz with a potential amplitude of 10 mV. The working electrode was prepared as follows; 2 mg of nanocomposite, 20 µL of Nafion solution (5 wt%) and 400 µL of isopropanol were mixed and ultrasonicated at 27°C for 2 h. The 30 µL of the prepared slurry was deposited on the active area of the glassy carbon electrode and dried at 80°C for 30 minutes to evaporate the isopropanol.

3. Results and Discussion

The $MnO_2/ACs_{(X:Y)}$ nanocomposites with different MnO_2 loading were prepared and the physicochemical characteristics

Table 1. BET pore characteristics and EDS elemental compositions of ACs and its MnO_2-composites.

Samples	BET analysis			EDS (wt%)			
	S_{BET} (m^2/g)	D_{aver} (nm)	V_{pore} (cm^3/g)	C	O	S	Mn
Pure ACs	1318.4	2.40	0.79	85.69	12.05	2.06	-
$MnO_2/ACs_{(1:2)}$	106.8	7.14	0.19	42.12	21.78	1.94	34.17
$MnO_2/ACs_{(1:1)}$	636.0	3.41	0.39	45.51	21.58	2.48	30.43
$MnO_2/ACs_{(1:2)}$	600.2	2.60	0.54	60.62	23.52	2.37	13.49
$MnO_2/ACs_{(1:4)}$	1355.7	2.38	0.81	72.44	15.38	2.07	10.11
$MnO_2/ACs_{(1:8)}$	1519.3	2.51	0.95	77.33	15.65	2.46	4.57
$MnO_2/ACs_{(1:10)}$	1560.9	2.35	0.92	77.87	14.23	2.72	5.18
$MnO_2/ACs_{(1:12)}$	**1597.4**	**2.55**	**1.02**	**79.73**	**12.38**	**3.17**	**4.72**
$MnO_2/ACs_{(1:14)}$	1705.3	2.68	1.14	81.73	12.12	2.28	3.87
$MnO_2/ACs_{(1:16)}$	1641.4	2.00	0.82	85.12	10.16	2.53	2.19

were investigated in detail. The representative data of SEM-EDS, BET, Raman, XRD and XPS obtained for pure ACs and $MnO_2/ACs_{(1:12)}$ are shown and discussed. Data of other samples [$MnO_2/ACs_{(X:Y)}$] are given in the EIS (Fig. S1-S4). The BET pore properties and EDS elemental compositions of ACs and nanocomposites are presented Table 1. Fig. 1 represents the EDS weight percentage of elements (C, O, S and Mn) presented in $MnO_2/ACs_{(1:12)}$ nanocomposites. As expected, the pure ACs showed 0% of Mn with C (85.69%), O (12.50%) and S (2.06%). Although the presence of N was detected by XPS analysis, the EDS result didn't show any peak corresponds to N which may be due to the presence of a trace amount of N. In case of $MnO_2/ACs_{(X:Y)}$ nanocomposites, the wt% of Mn was gradually increased with increasing $KMnO_4$ ratio (Table 1). Fig. 2 shows the representative SEM image, EDS spectrum and its corresponding elemental mappings (C, Mn and O) of $MnO_2/ACs_{(1:12)}$. The weight percentage of Mn, O, S and C in $MnO_2/ACs_{(1:12)}$ nanocomposites was found to be 4.72, 12.38, 3.17 and 79.73, respectively. In addition, homogeneous dispersion of MnO_2 was confirmed by the elemental mapping of Mn [Fig. 2(iii)]. For more details, refer Fig. S1 in EIS. Fig. 3 represents nitrogen adsorption–desorption isotherms of pure ACs and $MnO_2/ACs_{(1:12)}$. The pure ACs showed the specific

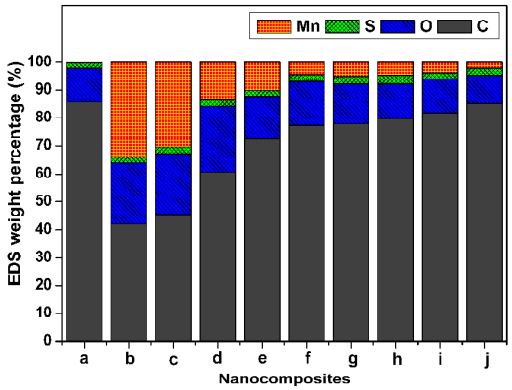

Fig. 1 EDS elemental weight percentage of (a) pure ACs, (b) $MnO_2/ACs_{(1:2)}$, (c) $MnO_2/ACs_{(1:1)}$, (d) $MnO_2/ACs_{(1:2)}$, (e) $MnO_2/ACs_{(1:4)}$, (f) $MnO_2/ACs_{(1:8)}$, (g) $MnO_2/ACs_{(1:10)}$, (h) **$MnO_2/ACs_{(1:12)}$,** (i) $MnO_2/ACs_{(1:14)}$, and (j) $MnO_2/ACs_{(1:16)}$.

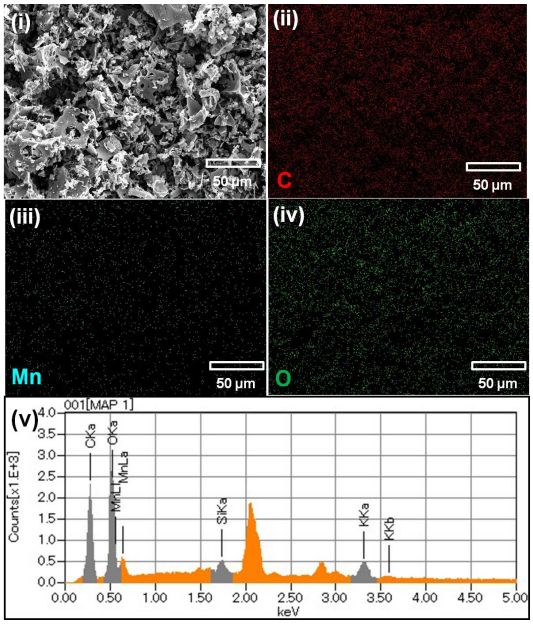

Fig. 2 (i) SEM image of $MnO_2/ACs_{(1:12)}$ and corresponding elemental mapping of (ii) C, (iii) Mn and (iv) O. (v) EDS spectrum of $MnO_2/ACs_{(1:12)}$.

surface area of 1318.4 m^2 g^{-1}. Alike, the BET surface areas of 1597.4 m^2g^{-1} was observed for $MnO_2/ACs_{(1:12)}$. In addition, the $MnO_2/ACs_{(1:12)}$ has total pore volume and average pore diameter of 1.02 cm^3 g^{-1} and 2.5542 nm, respectively (Table 1). This high surface area can offer a sufficient electrode/electrolyte interface for ion or charge accumulation. Moreover, the presence of high volume of pores (1.02 cm^3 g^{-1}) in the materials can assist for the rapid diffusion of ions and results in a remarkably improved rate performance of electrode materials [20].

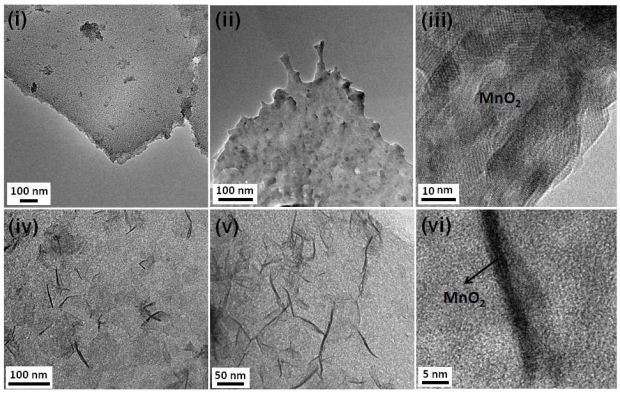

Fig. 3 HR-TEM images of (i) ACs, (ii and iii) $MnO_2/ACs_{(1:2)}$ and (iv-vi) $MnO_2/ACs_{(1:12)}$ [Images iii and vi are magnified images of $MnO_2/ACs_{(1:2)}$ and $MnO_2/ACs_{(1:12)}$, respectively].

The HR-TEM images were taken to study the microstructure of the ACs [Fig. 3(i)], $MnO_2/ACs_{(1:2)}$ [Fig. 3(ii and iii)] and $MnO_2/ACs_{(1:12)}$ [Fig. 3(iv-vi)]. As seen from HR-TEM images of pure ACs in Fig. 3(i), the architecture of ACs with

two-dimensional (2D) nanosheet morphology and the average thickness of the sheets were calculated to be ~65 nm. In addition, meso/micropores channels can be clearly seen on the surface of the nanosheets. In Fig. 3, the $MnO_2/ACs_{(X:Y)}$ composite showed that the needle like MnO_2 was homogeneously anchored on the 2D nanosheet. The average diameter and average length of the MnO_2 needles are found to be ~14 nm and ~110 nm, respectively. Interestingly, the average thickness of the nanosheets was dramatically decreased from 65 to 41 nm compared to pure ACs. In general, the inter-layers of carbon stacked by van der Waals forces have interaction energy of ~2 eV/nm^2 and typically a very weak ~300 nN/lm^2 magnitude of force is required to break this energy [21, 22]. In the present study, the exfoliation of the carbon sheets might have achieved during the preparation of nanocomposite (stirring and sonication process). In addition, the formed MnO_2 may be stabilized or prevented the carbon nanosheets from the further regeneration. The HR-TEM result agrees well with the BET results. Moreover, it was found that the loading of $KMnO_4$ has greater influence on the structure of the MnO_2. At higher loading of MnO_2, the surface morphology of the nanocomposites was quite different and no needle-like MnO_2 structures were observed on the carbon nanosheets. Instead, the MnO_2 was fully covered the carbon sheets at higher loading of $KMnO_4$. The needle-like nanostructure of MnO_2 is can help to an easy ionic charge transport at electrode/electrolyte interfaces [23].

XRD and Raman spectra were recorded to further investigate the graphitic structure [ordered and disordered (defect sites) nature] of pure ACs and nanocomposites (Figs. 4, 5, S3 and S4). Fig. 4 shows the XRD patterns of pure ACs and $MnO_2/ACs_{(1:12)}$. Two characteristic peaks were seen at around 2ϑ = 22.3° corresponding to (002) and 2ϑ = 43.8° (a weak peak) corresponding to (101) plane [24]. The XRD peak at around 2ϑ = 22.3° (002) attributed to a well-defined graphitic stacking. Alike, the weak peak at 2ϑ = 43.8° supports to the higher degree of interlayer condensation of carbon. Moreover, the clear observation of these XRD peaks indicating that the pure ACs and $MnO_2/ACs_{(1:12)}$ consist of small domains of prearranged graphene sheets. These results support that the samples are highly conductive in nature [25]. Raman spectra of

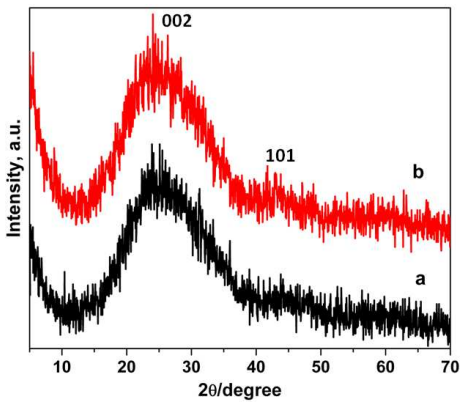

Fig. 4 XRD spectra of ACs (a) and $MnO_2/ACs_{(1:12)}$ (b).

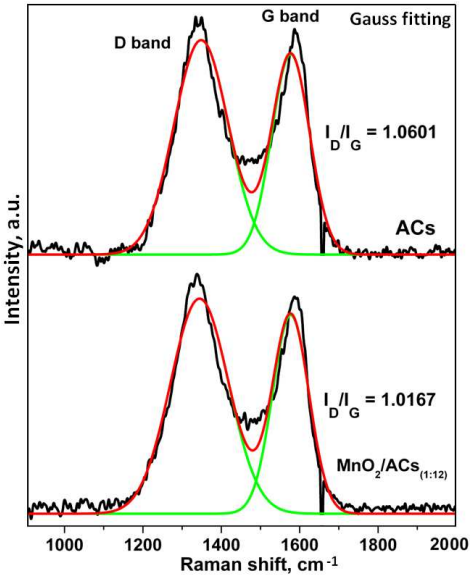

Fig. 5 Raman spectra of ACs (a) and $MnO_2/ACs_{(1:12)}$ (b).

both ACs and $MnO_2/ACs_{(1:12)}$ showed two characteristic bands at 1325 (D band) and 1597 cm^{-1} (G band) [26]. The G-band was invented from the in-plane vibration of sp^2 carbon atoms, which attributed to the graphitic carbon. The D-band line was related to the amount of disorder, indicating the presence defect sites in the carbon network. Generally, the D/G ratio of band intensities is often used to study defects concentration in carbon [27]. At first, the D band and G band were fitted as the sum of a Gaussian function and then the I_G/I_D values were calculated (Fig. 5). The I_G/I_D values of ACs and $MnO_2/ACs_{(1:12)}$ were calculated to be 1.0167 and 1.0601, respectively. The Raman I_G/I_D values confirm a highly graphitized ACs and $MnO_2/ACs_{(1:12)}$, offering an excellent electric conductivity, which is consistent with the XRD results [28].

Further, the XPS spectra were recorded for pure ACs and $MnO_2/ACs_{(1:12)}$. Fig. 6 shows the high-resolution XPS spectra of C1s, N1s, O1s, S2p, and Mn2p. In was confirmed that the chemical compositions of pure ACs and nanocomposites are consist of C, N, O and S. The narrow and intense C 1s XPS peak was observed for both ACs and $MnO_2/ACs_{(1:12)}$, indicating an improved degree of graphitic order. Alike, the O 1s peak located at B.E. = 533.5 eV shows the presence of oxygen atoms. In fact the oxygen functional groups can enhance wettability of the carbon materials [29]. A strong and broad peak at B.E. = 400 eV (N 1s XPS peak) was observed which reveal the presence of N species in the form of pyridinic, pyrrolic, N-oxide and quaternary nitrogen [30]. Similarly, the S appears at approximately B.E. = 165 eV. In fact the presence of heteroatom such as S, N and O can contribute greatly to the pseudocapacitance. Two obvious peaks at B.E. = 642.0 eV and B.E. = 653.8 eV are observed in the Mn 2p XPS spectrum, corresponding to Mn $2p_{3/2}$ and Mn $2p_{1/2}$ peak, respectively. The B.E. values of Mn 2p peaks confirmed the +4 oxidation state of Mn in $MnO_2/ACs_{(1:12)}$ [31].

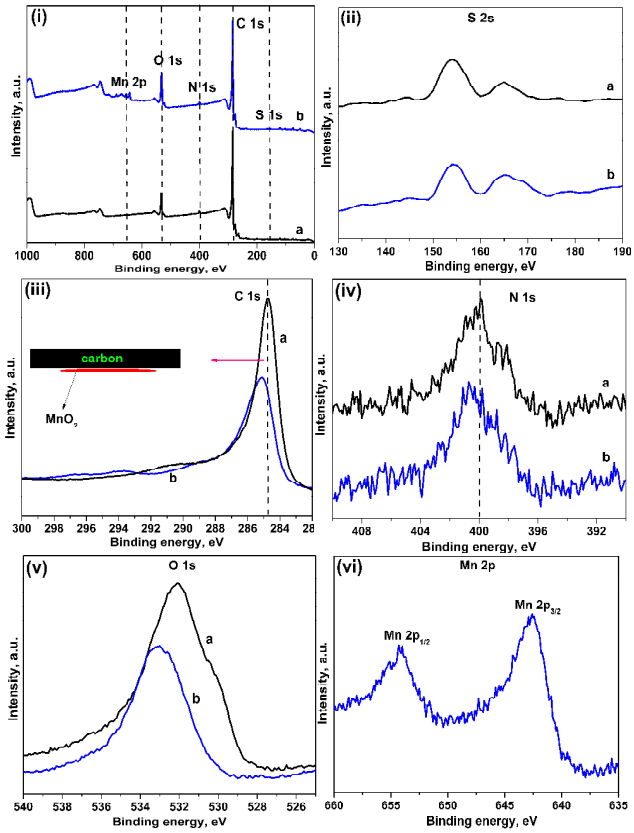

Fig. 6 (i) Survey XPS spectra, (ii) S 2s peaks, (iii) C 1s peaks, (iv) N 1s peaks and, (v) O 1s peaks of ACs (a) and $MnO_2/ACs_{(1:12)}$, and (vi) XPS Mn 2p peak of $MnO_2/ACs_{(1:12)}$.

To evaluate the specific capacitance (Cs) of the prepared ACs and nanocomposites, CV curves were recorded at different scan rates in three different electrolytes such as 1.0 M KOH, 1.0 M H_2SO_4, and 1.0 M Na_2SO_4; the results are presented in

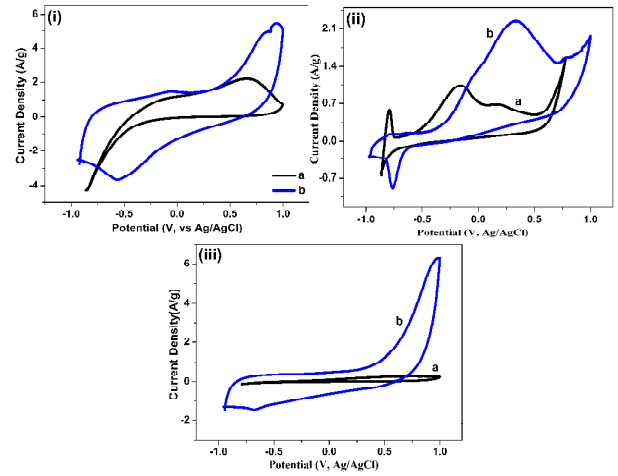

Fig. 7 Cyclic voltammetry measurements of pure ACs (a) and $MnO_2/ACs_{(1:12)}$ (b) in (i) 1.0 M H_2SO_4, (ii) 1.0 M KOH and (iii) 1.0 M Na_2SO_4 over a potential range from -1.0 to 1.0 V at a scan rate of 5 mV s^{-1}.

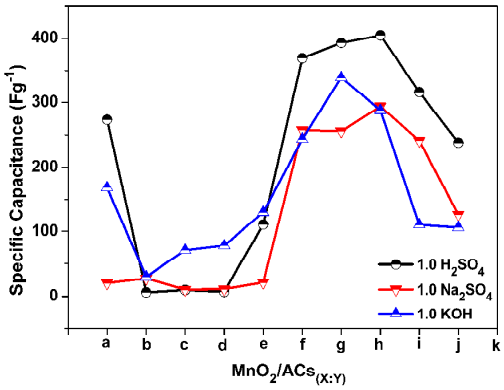

Fig. 8 Specific capacitances of (a) pure ACs, (b) $MnO_2/ACs_{(1:2)}$, (c) $MnO_2/ACs_{(1:1)}$, (d) $MnO_2/ACs_{(1:2)}$, (e) $MnO_2/ACs_{(1:4)}$, (f) $MnO_2/ACs_{(1:8)}$, (g) $MnO_2/ACs_{(1:10)}$, (h) **$MnO_2/ACs_{(1:12)}$**, (i) $MnO_2/ACs_{(1:14)}$, and (j) $MnO_2/ACs_{(1:16)}$ at scan rate of 5 mV S^{-1}.

Figs. 8 and 9. As can be seen in Fig. 7, the shape of the CV curves is slightly distorted from the rectangular shape. The polarization resistance of the samples is the main reason for the distortion of CV curves [32]. In addition, the presence of functional groups contributes to the pseudocapacitance behavior and the appearance of wide redox peak [33]. Fig. 8 shows the calculated Cs values of ACs and nanocomposites at scan rate of 5 mV s^{-1}. The superior capacitance performance of $MnO_2/ACs_{(X:Y)}$ was realized from the higher Cs values in all the three different electrolytes. At the scan rate of 5 mV s^{-1}, the $MnO_2/ACs_{(1:12)}$ achieved a maximum Cs of 410 F/g, 345 F/g and 291 F/g in 1.0 M H_2SO_4, 1.0 KOH and 1.0 Na_2SO_4, respectively. However, under same conditions, the pure ACs showed the Cs values of 275 F/g, 171 F/g and 22 F/g in 1.0 M H_2SO_4, 1.0 KOH and 1.0 Na_2SO_4, respectively. In comparison to pure ACs, the better Cs of $MnO_2/ACs_{(1:12)}$ is due to the presence of MnO_2. In fact, the charge can store on both MnO_2 and ACs support, and therefore, the better Cs has been achieved [34]. To the best of our knowledge, this is the first MnO_2-based carbon nanocomposite to show good Cs in three kinds of electrolytes. Effect of MnO_2 loading on electrochemical performance was also investigated. Fig. 8 represents the Cs values of nanocomposites with different MnO_2 loading. As can be seen in Fig. 8, the loading of MnO_2 has a profound effect on the electrochemical performance of the $MnO_2/ACs_{(1:12)}$. At higher loading of MnO_2 [such as $MnO_2/ACs_{(1:2)}$], the MnO_2 has played a negative role by blocking the carbon surface and hinder the transport of ions [35]. In addition, the blocking of interconnected pores of the carbon support by the MnO_2 leads to a lower surface area of the nanocomposites and, therefore, the lower Cs values are obtained. Alike, very low MnO_2 loadings also exhibited low Cs values which may be due to the insufficient amount of MnO_2 [36]. This result agrees well with the BET results.

Further, the Cs of pure ACs and $MnO_2/ACs_{(1:12)}$ at different scan rates was measured in 1.0 H_2SO_4; the results are presented in Fig. 9. It was noticed that the Cs values are gradually decreased with scan rate for both ACs and $MnO_2/ACs_{(X:Y)}$. At the scan rate of 500 mV s^{-1}, the ACs showed

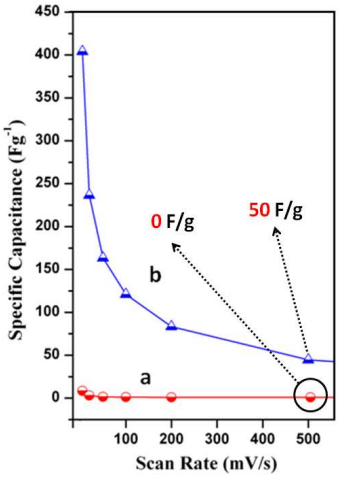

Fig. 9 Specific capacitance of (a) pure ACs and $MnO_2/ACs_{(X:Y)}$ at different scan rates determined in 1.0 H_2SO_4.

nearly zero capacitance, whereas, the $MnO_2/ACs_{(1:12)}$ maintained a maximum Cs of about 50 F/g. The EIS spectrum [Fig. 10(i)] of ACs and $MnO_2/ACs_{(1:12)}$ presented a depressed semicircle and a smaller interfacial charge-transfer resistance, representing good conductivity of the materials and high ion transfer speed across interfaces between the electrolyte and electrode [37]. Fig. 10(ii) represents the cycle stability of pure ACs and $MnO_2/ACs_{(1:12)}$ at scan rate of 5 mV s^{-1} in 1.0 M H_2SO_4.

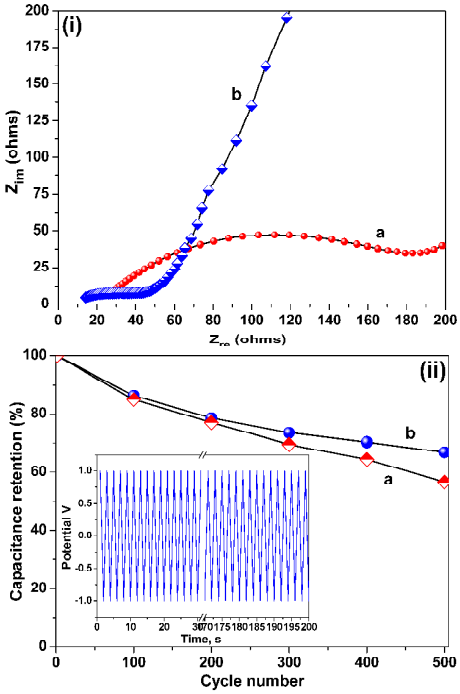

Fig. 10 (i) Nyquist plots of (a) pure ACs and $MnO_2/ACs_{(X:Y)}$ recorded in 1.0 M H_2SO_4 and (ii) cycle stability of pure ACs (a) and $MnO_2/ACs_{(X:Y)}$ (b) in 1.0 M H_2SO_4; Inset: galvanostatic charge–discharge cycles.

It was calculated that about 70% of the Cs was maintained by the $MnO_2/ACs_{(1:12)}$ after 500 cycles. The result confirms the good capacitance retention of the electrode material. However, after 500 cycles, the Cs of pure ACs was decreased to 59%. Overall, the better performance of the $MnO_2/ACs_{(X:Y)}$ is due five obvious reasons (i) the high specific surface area, (ii) high average pore size and mean pore volume, (iii) the presence of heteroatom such as O, S and N, (iv) conductivity of carbon and (v) needle-like MnO_2.

Table 2. Comparison of the capacity for different MnO_2-based electrode materials

nanocomposites	Cs F/g	scan rate mV s^{-1}	reference
$MnO_2/ACs_{(1:12)}$	410 (1.0 H_2SO_4) 345 (1.0 KOH) 291 (1.0 Na_2SO_4)	5	this work
graphene–MnO_2	310	2	[16]
MnO_2/activated CNTs	250	10	[38]
C/ MnO_2 nanorods	165	5	[17]
MnO_2/ACs	62	-	[39]
MnO_2/aniline	626	10	[40]
MnO_2-VACNF	437	1	[41]
MnO_2/diamond	326	10	[42]
flexible carbon cloth based MnO_2 nanosheets	683.73	-	[42]
ternary MnO_2/graphene nanosheets/CNTs composite	367	20	[44]
MnO_2 / carbon spheres	412	2	[45]

The Cs performance of the present $MnO_2/ACs_{(1:12)}$ is better or comparable to many other MnO_2-based electrode materials (see Table 2) including graphene–MnO_2, MnO_2/activated CNTs, C/MnO_2 nanorods, MnO_2/ACs, MnO_2/aniline, MnO_2-VACNF, MnO_2/diamond, flexible carbon cloth based MnO_2 nanosheets, ternary MnO_2/graphene nanosheets/CNTs composites, and MnO_2 nanocrystals/carbon spheres.

4. Conclusions

In summary, needle-like MnO_2 with different weight percentage was successfully decorated on ACs by a simple wet impregnation method. The physicochemical properties of the prepared nanocomposites were characterized in detail. For the first time, we demonstrated the MnO_2-based carbon nanocomposite as electrode materials for supercapacitor in three different electrolytes (1.0 M H_2SO_4, 1.0 M KOH and 1.0 M Na_2SO_4). The nanocomposites were worked well as electrode materials for supercapacitors. Interestingly, the

MnO_2/ACs achieved a maximum capacitance of 410 F/g, 345 F/g and 291 F/g in 1.0 M H_2SO_4, 1.0 KOH and 1.0 Na_2SO_4, respectively. Moreover, the $MnO_2/ACs_{(1:12)}$ showed capacitance of ~300 F/g even after 500 cycles in 1.0 M H_2SO_4.

Notes and references

1 P. Simon, Y. Gogotsi, *Nat. Mater.*, 2008, **7**, 845.
2 D. N. Futaba, K. Hata, T. Yamada, T. Hiraoka, Y. Hayamizu, Y. Kakudate, O. Tanaike, H. Hatori, M. Yumura, S. Iijima, *Nat. Mater.*, 2006,**5**, 987.
3 L.F. Chen, X.D. Zhang, H.W. Liang, M. Kong, Q.F. Guan, P. Chen, Z.Y. Wu, S.H. Yu, *ACS Nano,* 2012, **6** , 7092.
4 H.P. Cong, X.C. Ren, P. Wang, *Chem. Soc. Rev.,* 2009,**38**, 2520.
5 W. Qian, F. Sun, Y. Xu, L. Qiu, C. Liu, S. Wang, F. Yan, *Energy Environ. Sci.*, 2014, **7**, 379.
6 G. Ma, D. Guo, Q. Yang, X. Zhou, X. Zhao, Z.Q. Lei, *RSC Adv.*, 2015, **5**, 64704.
7 M. Biswal, A. Banerjee, M. Deo, S. Ogale, *Energy Environ. Sci.*, 2013, **6**, 1249.
8 C. Peng, X. Yan, R. Wang, J. Lang, Y. Ou, Q. Xue, *Electrochim. Acta*, 2013, **87**, 401.
9 J. Zhang, L. Gong, K. Sun, J. Jiang, X. Zhang, *J. Solid State Chem.*, 2012, **16**, 2179.
10 M. P. Bichat, E. Raymundo-Piñero, F. Beguin, *Carbon*, 2010, **48**, 4351.
11 H. Li, R. Wang, R. Cao, *Microporous Mesoporous Mater.*, 2008, **111**, 32.
12 K. Lota, A. Sierczynska, G. Lota, *Int. J. Electrochem.*, 2011, **2011**, 321473.
13 J. Jiang, A. Kucernak, *Electrochim Acta.*, 2002, **47**, 2381.
14 M. Toupin, T. Brousse, D. Belanger, *Chem. Mater.*, 2004, **16**, 3184.
15 G. Yu, L. Hu, N. Liu, H. Wang, M. Vosgueritchian, Y. Yang, Y. Cui, Z.Bao, *Nano Lett.*, 2011, **11**, 4438.
16 J. Yan, Z. Fan, T. Wei, W. Qian, M. Zhang, F. Wei, *Carbon,* 2010, **48**, 3825-3833.
17 R. K. Sharma, H. S. Oh, Y. G. Shul, H. Kim, *J. Power Sources*, 2007, **173**, 1024.
18 M. Zhi, C. Xiang, J. Li, M. Li, N. Wu, *Nanoscale*, 2013, **5**, 72-88.
19 J. P. Paraknowitsch, A. Thomas, *Energy Environ. Sci.*, 2013, **6**, 2839.
20 K. Lee, D. Kim, Y. Yoon, J. Yang, H. G. Yun, I. K. You, H. Lee, *RSC Adv.*, 2015, **5**, 60914.
21 Y. Zhang, J. P. Small, W. V. Pontius, P. Kim, *Appl. Phys. Lett.*, 2005, **86**, 073104.
22 M. Wu, G. A. Snook, G. Z. Chen, D. J. Fray, *Electrochem. Commun.*, 2004, **6**, 499.
23 M. Gopiraman, S.G. Babu, Z. Khatri, W. Kai, Y. A. Kim, M. Endo, R. Karvembu, I. S. Kim, *J. Phys. Chem. C.,* 2013, **117**, 23582.
24 M. Gopiraman, S.G. Babu, Z. Khatri, W. Kai, Y. A. Kim, M. Endo, R. Karvembu, I. S. Kim, *Carbon.* 2013, **62**, 135.
25 X. Li, G. Zhang, X. Bai, X. Sun, X. Wang, E. Wang, H. Dai, *Nat. Nanotechnol.,* 2008, **3**, 538.
26 A. Cuesta, P. Dhamelincourt, J. Laureyns, A. Martínez-Alonso1, J. M. D. Tascon, *Carbon*, 1994, **32**, 1523.
27 M. Gopiraman, R. Karvembu, I. S. Kim, *ACS Catal.* 2014, **4**, 2118.
28 L. Sun, C. Tian, Y. Fu, Y. Yang, J. Yin, L. Wang, H. Fu, *Chem. Eur. J.*, 2014, **20**, 564.
29 T. Tojo, K. Sakurai, H. Muramatsu, T. Hayashi, K. S. Yang, Y. Jung, C. M. Yang, M. Endo, Y. Kim, *RSC Adv.*, 2014, **4**, 62678.
30 T. C. Nagaiah, S. Kundu, M. Bron, M. Muhler, W. Schuhmann, *Electrochem. Commun.*, 2010, **12,** 338.
31 X. Lu, T. Zhai, X. Zhang, Y. Shen, L. Yuan, B. Hu, L. Gong, J. Chen, Y. Gao, J. Zhou, Y. Tong. Z. Wang. *Adv. Mater.,* 2012, **24**, 938.
32 R. Jiang, T. Huang, Y. Tang, J. Liu, L. Xue, J. Zhuang, A. Yu. *Electrochim. Acta*, **2009**, **54,** 7173.
33 X. Fan, Y. Lu, H. Xu, X. Kong, J. Wang, *J. Mater. Chem.*, 2011, **21**, 18753.
34 S. Ghasemi, R. Hosseinzadeh, M. Jafari, *Int. J. Hydrogen Energy*, 2015, **40**, 1037.
35 Y. He, W. Chen, X. Li, Z. Zhang, J. Fu, C. Zhao, E. Xie, *ACS Nano,* 2013, **7**, 174.
36 Y. Peng, Z. Chen, J. Wen, Q. Xiao, D. Weng, S. He, H. Geng, Y. Lu, *Nano Res.*, 2011, **4**, 216.
37 D. Antiohos, K. Pingmuang, M. S. Romano, S. Beirne, T. Romeo, P. Aitchisonc, A. Minett, G. Wallacea, S. Phanichphant, J. Chen, *Electrochim. Acta*, 2013, **101**, 99.
38 J. M. Ko, K. M. Kim, *Mater. Chem. Phys*., 2009, **114**, 837.
39 A. Yuan, Q. Zhang, *Electrochem. Commun.*, 2006, **8**, 1173.
40 R. I. Jafri, A. K. Mishra, S. Ramaprabhu, *J. Mater. Chem.*, 2011, **21**, 17601.
41 S. A. Klankowski, G. P. Pandey, G. Malek, C. R. Thomas, S. L. Bernasek, J. Wub, J. Li, *Nanoscale*, 2015, **7**, 8485.
42 S. Yu, N. Yang, H. Zhuang, J. Meyer, S. Mandal, O. A. Williams, I. Lilge, H. Schoonherr, X. Jiang, *J. Phys. Chem. C*, 2015, 10.1021/acs.jpcc.5b04719.
43 S. He, W. Chen, *J. Power Sources*, 2015, **294**, 150.
44 M. Ramezani, M. Fathi, F. Mahboubi, *Electrochim. Acta*, 2015, **174**, 345.
45 X. Wang, X. Fan, G. Li, M. Li, X. Xiao, A. Yu, Z. Chen, *Carbon*, 2015, **93**, 258.